Journal of Alloys and Compounds 927 (2022) 167005

Contents lists available at ScienceDirect

Journal of Alloys and Compounds

journal homepage: www.elsevier.com/locate/jalcom

Research Article

The effect of the Nb concentration on the corrosion resistance of nitrogen-containing multicomponent TiZrTaNb-based films in acidic environments

Eirini-Maria Paschalidou[a,*,1], Rui Shu[b,1], Robert Boyd[b], Athanasios A. Papaderakis[c], Babak Bakhit[b], Arnaud le Febvrier[b], Grzegorz Greczynski[b], Per Eklund[b], Leif Nyholm[a]

[a] Uppsala University, Department of Chemistry – Ångström Laboratory, Uppsala University, SE-751 21 Uppsala, Sweden
[b] Thin Film Physics Division, Department of Physics, Chemistry, and Biology (IFM), Linköping University, Linköping SE-581 83, Sweden
[c] Department of Chemistry and Henry Royce Institute, University of Manchester, Manchester M13 9PL, United Kingdom

ARTICLE INFO

Article history:
Received 24 May 2022
Received in revised form 14 August 2022
Accepted 27 August 2022
Available online 30 August 2022

Keywords:
Thin films
Multicomponent
Corrosion resistance
Passivation

ABSTRACT

Multicomponent as well as high-entropy-based nitrides have received increasing interest in the field of materials science and engineering. The structural characteristics of these compounds result in a mix of covalent, metallic, and ionic bonds that give rise to a number of attractive properties including high hardness, electrical and thermal conductivities as well as chemical stability. These properties render these materials promising candidates for various industrial applications involving harsh operating conditions. Herein, the corrosion resistances of dc magnetron sputtered nitrogen-containing $TiZrTaNb_y$ thin films with Nb content ranging from 8.0 to 24.5 at% have been investigated to provide insights regarding the corrosion resistances of multicomponent systems containing more than one passive element. The corrosion resistances and anodic behavior of the films were examined by electrochemical means in 0.1 M H_2SO_4 and 0.1 M HCl solutions. The results demonstrate that despite the significant differences in the concentration of one of the two main passive elements in the films i.e., Nb, the corrosion resistance did not differ significantly between the films. To provide insights into this phenomenon, the surface chemical state and composition of the prepared films were probed using X-ray photoelectron spectroscopy. It was shown that all samples exhibited Ta-rich surfaces after positive polarization up to 3.0 V vs. Ag/AgCl (3 M NaCl) as a result of the anodic dissolution of Zr and Ti. The thickness of the oxide layer formed upon different anodic polarization was studied using transmission electron microscopy, while complementary electrochemical impedance studies were performed. The extent of Nb dissolution from the surface of the films was, on the other hand, found to be small. These findings highlight the dominant role of Ta in the passivation of the films and demonstrate the minor effect of Nb concentration on the corrosion resistances of the films. However, it was demonstrated that the presence of Nb was still important for the corrosion resistance of the films above 1.4 V vs. Ag/AgCl (3 M NaCl), when replacing Nb with Cr, due to transpassive dissolution of Cr. These results facilitate the design of highly corrosion resistant multicomponent nitrides containing more than one passive element.

1. Introduction

Even though the corrosion field attracts a lot of attention, many corrosion problems remain unsolved due to difficulties with understanding fundamental issues about passivation. Passivity is one of the major factors that slows down the corrosion process. Some metals such as Nb and Ta, show high corrosion resistances and remain in a passive state even at potentials above 2.0 V vs. SHE in acidic environments [1]. In contrast, other metals, such as Cr and Mo, which are typical elements that are added to increase the corrosion resistance of steel, do not exhibit passivity above 1.0 V vs. SHE [2,3]. According to percolation theory, passivity in an alloy can be achieved when a minimum concentration of a passive element is present, referred to as the percolation threshold [4–6]. For example, in a stainless-steel alloy, the minimum concentration of the passive element Cr is about 12–13 at% [4–6], because of the need for a

* Corresponding author.
E-mail address: maria.paschalidou@kemi.uu.se (E.-M. Paschalidou).
[1] These authors contributed equally to the work.

https://doi.org/10.1016/j.jallcom.2022.167005

Table 1
Target powers used during the depositions as well as the elemental compositions and thicknesses for the $TiZrTaNb_y$ thin films.

Material system	y	Target power (W)				Composition (± 1.0 at%, EDS)				Thickness (± 10 nm)	
		Ti	Zr	Ta	Nb	Ti	Zr	Ta	Nb	N	
$TiZrTaNb_yN_x$	0.13	154	115	83	68	18.4	17.5	19.5	8.0	36.5	512
	0.19	144	108	77.5	91	18.8	17.5	19.8	13.0	30.8	503
	0.25	134	100	71	115	16.9	16.4	17.4	16.9	32.4	505
	0.31	124	93	67	136	15.6	14.7	16.3	20.6	32.8	504
	0.37	114	85	62	159	14.3	13.3	14.9	24.5	33.1	500

sufficiently high Cr surface coverage facilitating Cr-O-Cr bonding [4–6]. Despite the vast number of studies on the corrosion behavior of several types of alloys reported in the literature, the percolation theory has so far been solely applied to binary systems such as Fe-Cr, Ni-Cr and Mg-Al [4–10]. No insights have consequently been provided regarding the application of the percolation theory to multicomponent alloys containing more than one passivating elements.

The passivation of metals such as Nb and Ta at significantly high potentials suggests that these metals can be used in multicomponent thin films such as high entropy nitrides (HENs) [11], to improve their corrosion resistances by extending the passive regions to higher potentials. High-entropy nitrides, constitute a large category of high-entropy ceramics [12]; the latter constitute a category of high entropy alloys (HEAs) [13], when p-elements (i.e., carbon, nitrogen, boron, oxygen) are added to a HEA composition, forming carbides, nitrides, borides and oxides which are frequently named as high-entropy ceramics [12]. HENs can exhibit combined properties of ceramics and metals, such as good electrical conductivity, as well as high hardness and toughness [14]. The corrosion resistances of HEN systems can be affected by parameters such as their microstructures [15,18] and their composition [14–17]. Alloying metal elements with different passivation behaviors could allow the design of high-entropy alloys and multicomponent ceramics for applications requiring high corrosion resistances. For example, in case of $TiNbZrTaN_x$, it has been found that a stable passive region up to 3.0 V vs. Ag/AgCl (3 M NaCl) in 0.1 M H_2SO_4 can be achieved for films with $x < 0.64$ [16]. It is worth emphasizing that the abovementioned anodic potential limit of effective passivation is higher than the thermodynamic upper potential limit of aqueous electrolytes, i.e., ca. 1.23 V vs. SHE under standard conditions, as well as those of most non-aqueous electrolytes. This characteristic (i.e., the high anodic potential limit) can render these multicomponent composites industrially attractive towards several applications including electrosynthesis [19], electrochemical energy conversion [20], storage [21] and advanced electronics [22].

Previous studies of TiTaNb medium entropy alloy (MEA) thin films in 0.5 M H_2SO_4 solution have shown an improved corrosion resistance compared to that of pure Ti due to the formation of a stable passive oxide layer upon positive polarization. In this oxide layer the concentrations of Nb and Ta were found to be higher than that of Ti [23]. Similar studies on equiatomic TiZr (Hf, Ta, Nb) MEAs support the idea that alloying with Ta and Nb can significantly improve the corrosion resistance of TiZr alloys [24].

The present study aims to provide insights regarding the corrosion resistances of multicomponent systems containing more than one passive element. Nitrogen-containing multicomponent TaTiZrNb composites were prepared using co-sputtering with single-element targets where Nb and Ta act as the passive elements. The effect of the Nb concentration on the corrosion resistance of the films was examined, while maintaining the Ta concentration constant. Ti and Zr were not considered as passive elements on the basis of their Pourbaix diagrams [1], which at pH= 1 predict that Zr should be present as ZrO^{2+} (zirconyl ion) above − 1.7 V vs. SHE, whereas Ti should be present as Ti^{2+} between − 1.8 and − 0.4 V vs. SHE, and as TiO_2 above − 0.4 V vs. SHE. The concentration of Nb in the films, given as the ratio between the Nb concentration and the total metal concentration in atomic percent, was varied from 0.13 to 0.37. To avoid fast etching at high potentials i.e., above 2.0 V vs. Ag/AgCl (3 M NaCl), the nitrogen concentration x was kept lower than 0.64 based on the findings of previous studies [16,17]. Films with nitrogen concentrations higher than 0.64 only featured a stable current plateau up to 2.0 V, indicating that the corrosion resistance depended on the nitrogen concentration in the films [16]. Overall, it is envisaged that this work will contribute significantly to the ongoing research on the design of highly corrosion resistant multicomponent nitrides containing more than one passive elements.

2. Experimental methods

Nitrogen-containing TiZrTaNb-based thin films were deposited on Si(100) substrates (size: 10 ×10 mm^2) using magnetron sputtering in an ultrahigh vacuum chamber (base pressure < 10^{-7} Pa) as described elsewhere [25] with elemental targets (Ti, Zr, Ta and Nb) with a diameter of 50.8 mm. The distance between the targets and the substrate holder was approximately 140 mm. The substrate holder was maintained at 400 °C and a constant rotation rate of 20 rpm. A substrate bias of − 100 V was applied during deposition. The total flow of the gas mixture of Ar and N_2 was kept at 65 sccm, corresponding to a total pressure of 0.47 Pa in the chamber. The flow ratio of reactive nitrogen, f_{rgas} = N_2/(Ar + N_2) was set to 4.1%. The discharge powers applied to the Ti, Zr and Ta targets were adjusted individually to achieve an equimolar composition. The nitrogen-containing $TiZrTaNb_y$ films were deposited under different target-power conditions. To control the Nb concentration and retain the concentrations of Ti, Zr, Ta, and nitrogen, the total applied power on the four targets was fixed at 420 ± 1 W, while the power of Nb target was varied from 68 to 159 W. The fraction of the Nb-target power with respect to the total power of the four targets was varied from 16% to 38%. The specific target power can be found in Table 1. Silicon (100) substrates (with a size of 10 × 10 mm^2) were cleaned sequentially with acetone and ethanol in an ultrasonic bath for 10 min each and finally blow-dried with nitrogen gas. The substrates were preheated for at least 30 min prior to each deposition to obtain a homogeneous temperature. The deposition time was 20 min for all the films.

The elemental compositions of the nitrogen-containing $TiZrTaNb_yN_x$ films were determined using energy-dispersive X-ray spectrometry (EDS, Oxford Instruments X-Max). The surface chemistry and elemental compositions in the surface region of the samples were studied by X-ray photoelectron spectroscopy (XPS) and performed with a Kratos Axis Ultra DLD instrument from Kratos Analytical (UK) employing monochromatic Al K_α radiation ($h\nu$ = 1486.6 eV). The corroded films were analyzed in the as-received (corroded) state, whereas the pristine films were measured before and after sputter-etching for 120 s with a 4 keV Ar^+ ion beam incident at 70° with respect to the sample normal. The XPS measurements were used to evaluate the surface chemistry of the samples before and after the corrosion tests. After this, the Ar^+ ion energy was decreased to 500 eV for 600 s to minimize surface damage. The binding energy (BE) scale of the spectrometer was

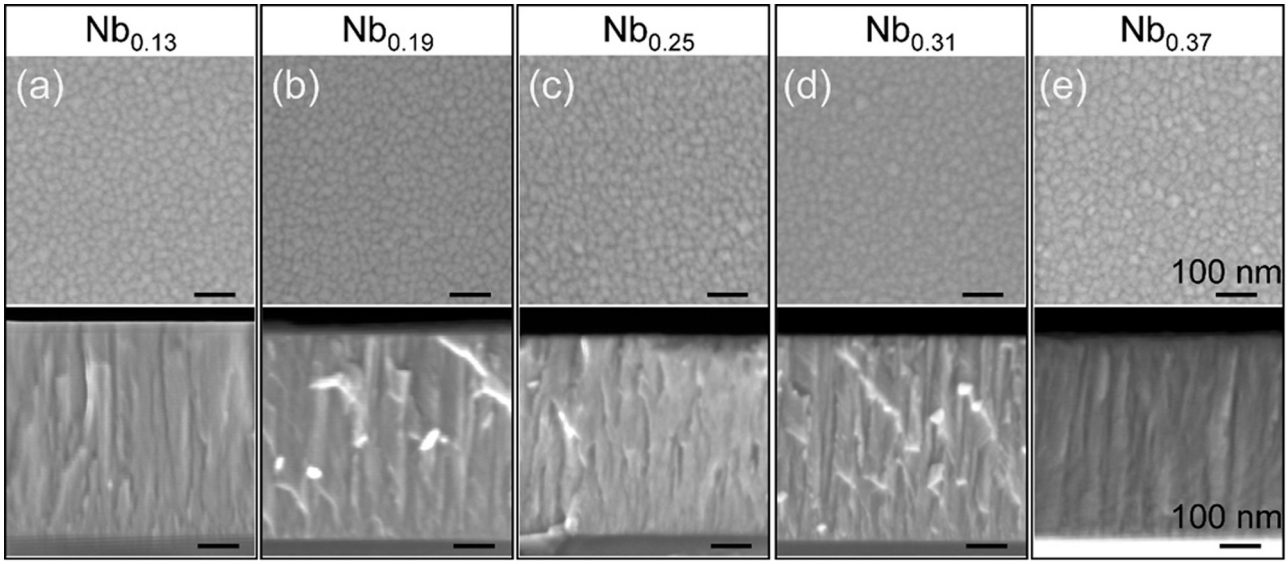

Fig. 1. SEM top-view (first row) and cross-section (second row) images of the $Nb_{0.13}$ (a), $Nb_{0.19}$ (b), $Nb_{0.25}$ (c), $Nb_{0.31}$ (d) and $Nb_{0.37}$ (e) thin films, respectively.

calibrated using the ISO-certified procedure [26]. The sample Fermi edge was used as an internal charge reference, to avoid problems related to the use of the C 1 s peak of the adventitious carbon [27]. The analyzer pass energy was set to 20 eV which resulted in the full width at half maximum of 0.55 eV for the Ag $3d_{5/2}$ peak, which is a typical calibration reference. Elemental quantification was performed using Casa XPS software (version 2.3.16), based upon the peak areas obtained from narrow energy range scans and the elemental sensitivity factors supplied by Kratos Analytical Ltd.

The crystal structure was evaluated by X-ray diffraction (XRD) measurements with a PANalytical X′Pert PRO diffractometer in a Bragg-Brentano geometry. Top-view and cross-section surface morphologies of the films were examined with a scanning electron microscope (SEM, Sigma 300, Zeiss, and a Merlin Zeiss), with an acceleration voltage between 2.0 and 5.0 kV. Transmission electron microscopy (TEM) characterization was conducted with a FEI Tecnai G2 TF20 UT instrument with a field emission gun operated at 200 kV. The cross-section of some selected samples was studied with TEM, before and after the linear sweep voltammetry (LSV) measurement. The samples were prepared individually using the following steps: firstly, they were glued onto a Ti grid, and then they were polished down to 50 µm thickness, followed by Ar^+-ion milling with a Gatan precision ion polishing system. Initially, the incident angle and energy of the Ar^+ ions were set at 5.5° and 4.0 keV, respectively. During the final step, the Ar^+ energy was decreased to 2.5 keV.

In the electrochemical experiments, a Teflon home-made three-electrode electrochemical cell was used in connection with an Autolab PGSTAT302N potentiostat/galvanostat (Metrohm Instruments). The thin films were used as the working electrodes and the electrical connection between the films and the potentiostat was made using copper tape. The Teflon cell had a 5 mm diameter opening at the bottom and the films were secured beneath this bottom opening, using a rubber O-ring between the film and Teflon cell. The area (0.2 cm^2) of the working electrode was delimited by an O-ring in the electrochemical cell. An Ag/AgCl (3.0 M NaCl) electrode and a Pt wire served as reference electrode and counter electrode, respectively. Prior to the experiments, the electrolytes (i.e., 0.1 M H_2SO_4 and 0.1 M HCl) were degassed with N_2 for about 45 min to remove the dissolved oxygen.

Polarization curves and electrochemical impedance spectroscopy (EIS) measurements were used to check the corrosion resistances of the thin films. Prior to the recording of the polarization curves, the films were left at the open circuit potential (OCP) for 45 min. The EIS measurements were conducted after 45 min at the OCP, and the impedance plots were recorded at the OCP value using a sinusoidal ac perturbation of 10 mV and a frequency range from 100 mHz to 100 kHz. The polarization curves were obtained with a scan rate of 1 mV/s, between − 0.7 and 3.0 V vs. Ag/AgCl (3 M NaCl). Moreover, two films with low (i.e., 0.19) and high (i.e., 0.37) Nb concentrations were subjected to a cathodic pre-treatment by applying a potential of − 1.0 V vs. Ag/AgCl (3 M NaCl) for three minutes before recording a polarization curve from − 0.7–3.0 V vs. Ag/AgCl (3 M NaCl). The purpose of this process was done to study if the cathodic pre-treatment had any impact on the electrochemical performances of the films. The values of the corrosion potential (E_{corr}) and corrosion current density (j_{corr}) were determined based on graphical extrapolations (i.e., Tafel plots) involving the anodic and cathodic current densities close to E_{corr} in the polarization curves. The films were washed twice with distilled water after each electrochemical experiment.

3. Results and discussion

3.1. Composition and morphology

The Nb concentration y in this study is defined as the ratio between the Nb concentration and the total metal concentration in atomic percent, which increased linearly from 0.13 to 0.37, corresponding to about 8–24.5 at% according to EDS (Table 1). Hereafter, these films will be referred as $Nb_{0.13}$, $Nb_{0.19}$, $Nb_{0.25}$, $Nb_{0.31}$ and $Nb_{0.37}$. The Ti, Zr and Ta metal concentrations in this series of films were nearly equimolar (± 2.0 at%). The nitrogen concentration in the films was varied between 30.8 at%, and 36.5 at%, as measured by EDS, indicating that all the nitrogen-containing $TiZrTaNb_yN_x$ films were substoichiometric in nitrogen with small differences between the films, given the high uncertainty associated with EDS measurements of nitrogen concentrations. The target power and atomic composition estimated by means of EDS measurements are given for each component in Table 1. Furthermore, all the films exhibited a similar NaCl-type fcc phase structure with a distinct (200) Bragg peak at ~41° (see Fig. S1 in the Supporting Information (SI)).

The top-view SEM images in Fig. 1 (first row), show that the thin films with different Nb concentrations all exhibited a surface morphology with fine grains with a diameter of ~20 nm. All thin films showed a dense nanocolumnar structure in the SEM cross-section

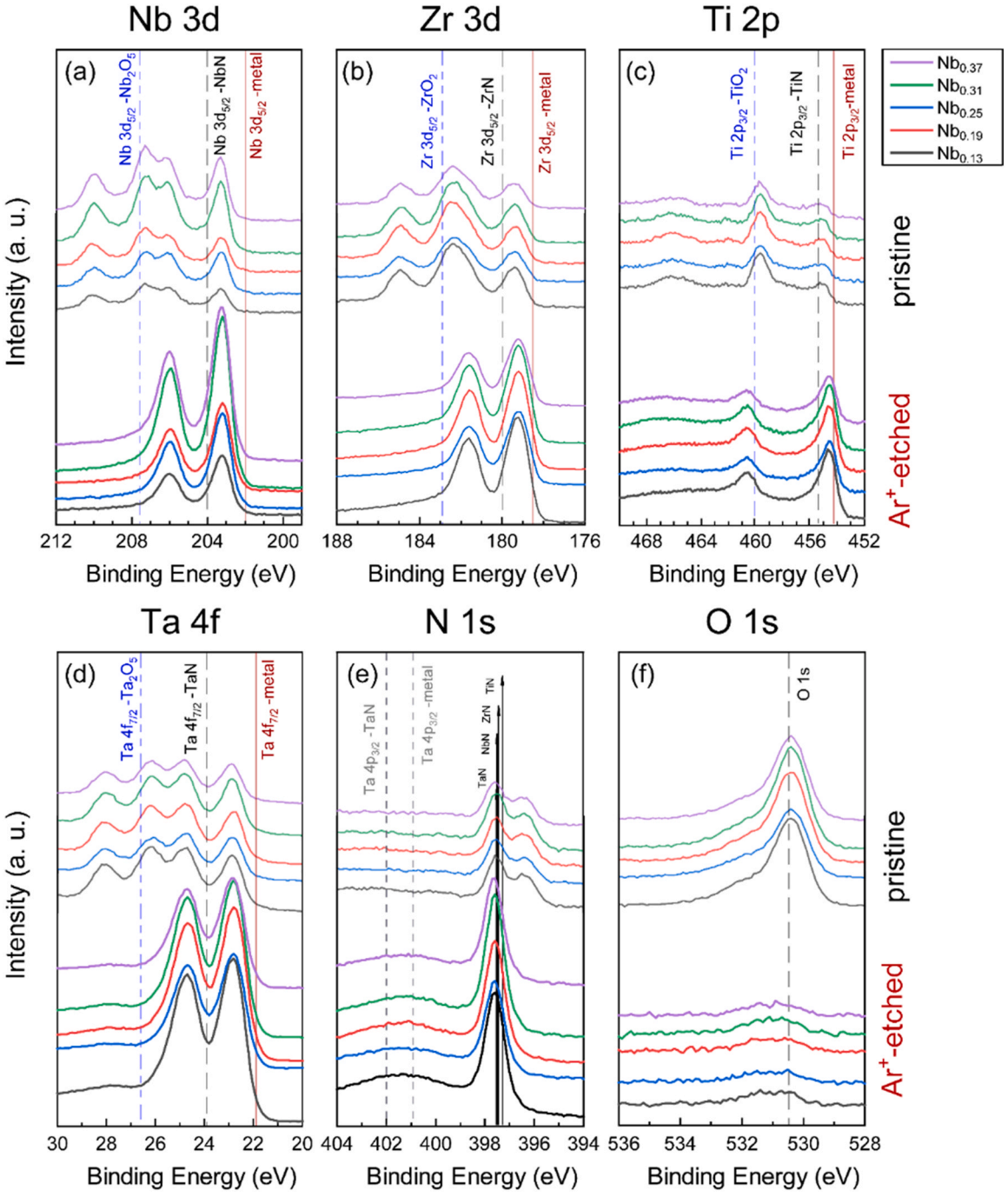

Fig. 2. High-resolution Nb 3d, Zr 3d, Ti 2p, Ta 4 f, N 1 s, and O 1 s XPS core level spectra recorded for the nitrogen-containing $TiZrTaNb_y$ films ($0.13 \le y \le 0.37$) using pristine films (first raw) and after sputter-etching (second raw), respectively. The vertical lines indicate the reference BE values for metals (red lines), oxides (blue dashed lines) and binary nitrides (grey dashed lines) [39].

images and an average thickness of ~500 nm (Fig. 1, second row). This microstructure of the films was optimized by substrate biasing based on the results of a previous study [28] as it was important to work with dense thin films in the corrosion studies. Previous corrosion studies on multicomponent AlCrNbYZrN thin films have shown that a higher corrosion resistance was observed for denser thin films [14]. As the surface microstructures were similar for all the films, although the Nb concentrations were different, the influence of the microstructure on the corrosion resistance of the films used in this study should hence have been negligible.

Fig. 2 shows high-resolution Nb 3d, Zr 3d, Ti 2p, Ta 4 f, N 1 s and O 1 s core-level spectra for the as-deposited films. The spectra were recorded without any surface-etching, and the results reveal that the surfaces of the films consisted of a mixture of oxides. The oxidation states of the constituting metals can be attributed to the presence of Nb_2O_5, ZrO_2, TiO_2, and Ta_2O_5, respectively. The BE positions for the primary oxide peaks were at 207.3 eV for Nb $3d_{5/2}$ of Nb_2O_5, at 182.3 eV for Zr $3d_{5/2}$ of ZrO_2, at 458.8 eV for Ti $2p_{3/2}$ for TiO_2 and at 26.1 eV for Ta 4 $f_{7/2}$ of Ta_2O_5, which were close to the reference values, i.e., 207.6 eV for Nb_2O_5 [29], 182.9 eV for ZrO_2 [30], 458.9 eV for TiO_2 [31], and 26.6 eV for Ta_2O_5 [32]. Since the XPS probing depth under present conditions was 6–7 nm [33], i.e., larger than the native oxide thickness (~2.7 nm, see Fig. 3a), the additional peaks corresponding to substoichiometric nitride states were also seen in the

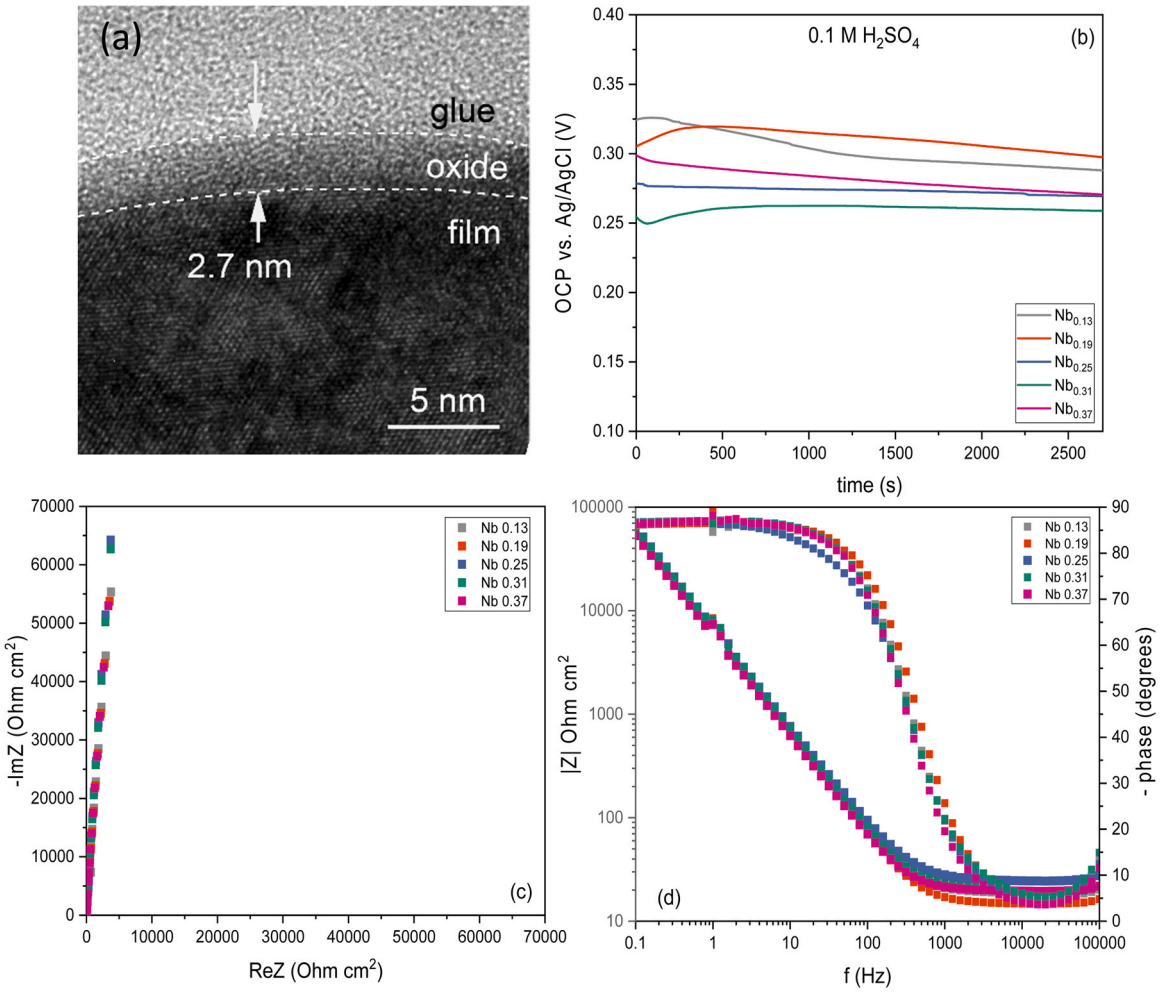

Fig. 3. (a) TEM image of the native oxide layer on a $Nb_{0.31}$ film. The average oxide thickness was about 2.7 nm. (b) The OCP as a function of time during 45 min in 0.1 M H_2SO_4. The Nyquist plots (c) as well as Bode plots (d) obtained in 0.1 M H_2SO_4 after 45 min at the OCP, for the $Nb_{0.13}$ (grey curve), $Nb_{0.19}$ (red curve), $Nb_{0.25}$ (blue curve), $Nb_{0.31}$ (green curve) and $Nb_{0.37}$ (purple curve) films.

core level spectra of the four metals. For these films, the BE values matched the BE values for the substoichiometric nitride peaks (in the bottom raw) after removing the native oxide by sputter-etching.

After Ar^+ etching Nb $3d_{5/2}$, Zr $3d_{5/2}$, and Ta $4f_{7/2}$ peaks shifted towards BE values typical for corresponding metals (marked with the red lines at 202.3 eV for Nb $3d_{5/2}$ [35], at 178.7 eV for Zr $3d_{5/2}$ [36], at 454.0 eV for Ti $2p_{3/2}$ [37] and 21.7 eV for Ta $4f_{7/2}$ [38]). XPS results after sputter etching also indicated that the studied films were substoichiometric with respect to nitrogen (rather than full nitrides) as the BE values were lower than the ones found for the binary nitrides used as references. This agrees with previous results [16] obtained for (TiZrTaNb)N_x films containing 30–36 at% of nitrogen.

3.2. Electrochemical experiments

3.2.1. OCP for 45 min and electrochemical impedance results in 0.1 M H_2SO_4 obtained prior to recording polarization curves

Prior to the recording of polarization curves, the films were immersed in the electrolyte under OCP conditions for 45 min. The OCP is a mixed potential based on the cathodic and anodic reactions taking place on the passive layer formed prior to this experiment. The thickness of the passive layer for a pristine $Nb_{0.31}$ film was estimated to be around 2.5–3.0 nm (Fig. 3a) using TEM. The OCP values were found to be about 0.26 V, 0.27 V, 0.27 V, 0.29 V and 0.30 V vs. Ag/AgCl (3 M NaCl) for the $Nb_{0.31}$, $Nb_{0.25}$, $Nb_{0.37}$, $Nb_{0.13}$ and $Nb_{0.19}$ films, respectively (Fig. 3b). For the films with different Nb concentrations, no significant differences were observed between the OCP values. In general, more positive potentials are associated with films that are more corrosion resistant. The fact that all studied films had similar OCP values indicates that the corrosion resistances were similar for all the films under OCP conditions. Nyquist (Fig. 3c) and Bode (phase and magnitude) plots (Fig. 3d) were obtained based on the EIS data recorded after immersing the films in the electrolyte for 45 min at the OCP. The qualitative features of the Nyquist plots were reminiscent of the ac response associated with a blocking (capacitive) interface. An almost constant real part was observed within the applied frequency range, with slight deviations seen at lower frequencies possibly arising by the introduction of frequency dispersion effects (i.e., surface inhomogeneities and/or kinetic dispersion effects). This behavior is close to the ideal capacitor case typically seen for corrosion-resistant films. In the phase Bode plots, the phase angles reached a plateau between ca. 85–87° below ca. 10 Hz for all films. The phase angle values were very close to 90°, as would be expected for a blocking interface, indicating a high corrosion resistance for all films under OCP conditions. This was attributed to the passive native oxide layers present on the surfaces of the films. Here it should, however, be noted that the XPS data presented in Fig. 2 show that passive films were already present on the surfaces of the pristine films. An additional noteworthy finding is that the electronic resistances of the films, estimated by the high frequency intercept of the Bode magnitude plots within the frequency range where the

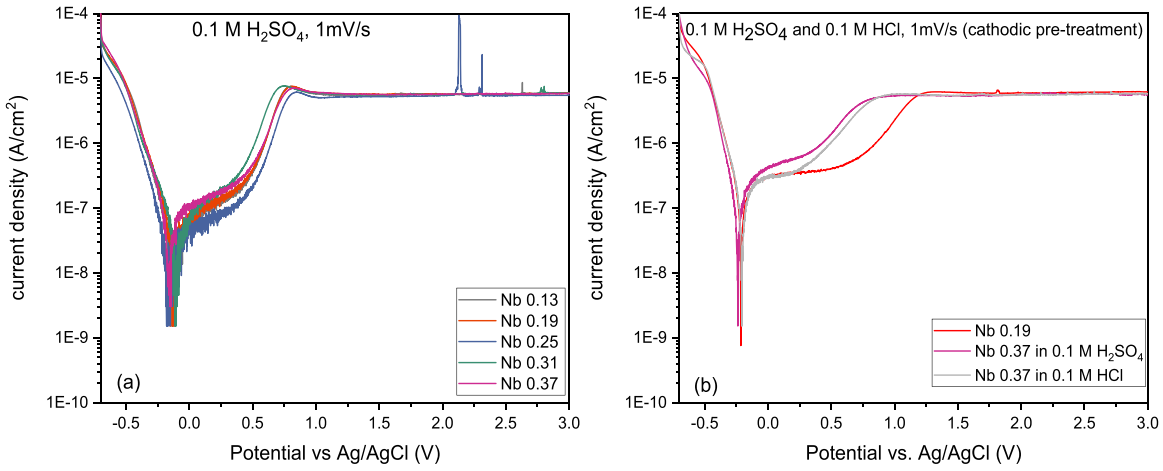

Fig. 4. (a) Polarization curves for the $TiZrTaNb_y$ nitrogen-containing films in 0.1 M H_2SO_4 recorded between − 0.7 and 3.0 V vs. Ag/AgCl (3 M NaCl) at room temperature and with a scan rate of 1 mV/s for the $Nb_{0.13}$ (grey curve), $Nb_{0.19}$ (red curve), $Nb_{0.25}$ (blue curve), $Nb_{0.31}$ (green curve) and $Nb_{0.37}$ (purple curve) films. (b) Analogous polarization curves for the $Nb_{0.19}$ and $Nb_{0.37}$ films recorded after a three-minute cathodic treatment at − 1.0 V vs. Ag/AgCl (3 M NaCl).

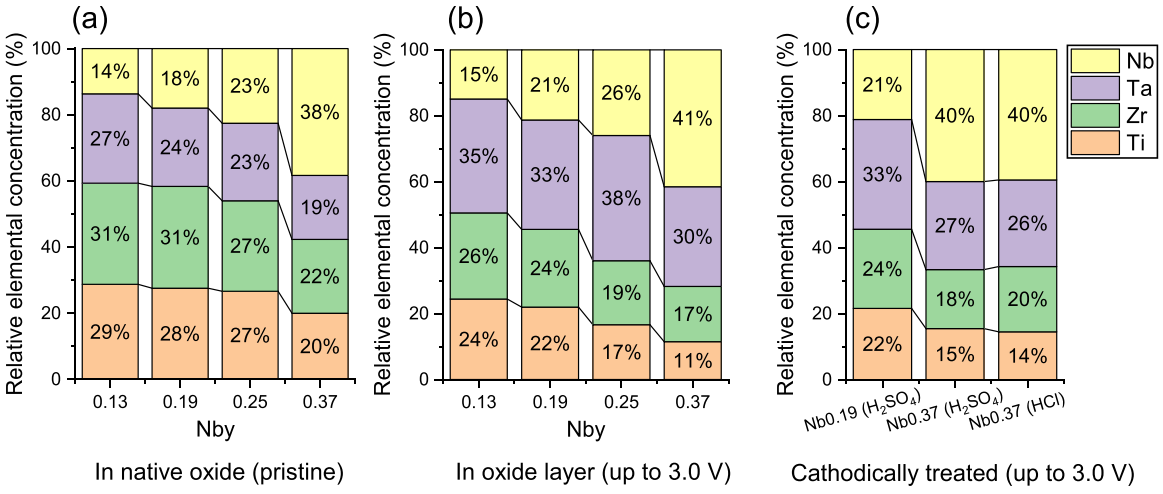

Fig. 5. Relative elemental concentrations obtained by peak-fitting the Nb 3d, Zr 3d, Ti 2p, Ta 4 f, XPS core level spectra recorded from the nitrogen-containing $TiZrTaNb_y$ films ($0.13 \le y \le 0.37$) in the pristine state (a) and after recording the polarization curves shown in Fig. 4a (b), and in Fig. 4b (c), respectively.

phase angle was less than 5° (a purely ohmic ac response can thus be justified due to a mixed contribution from electronic and electrolyte resistances) appeared not to depend significantly on the Nb concentration (Fig. S2). This indicates that the Nb concentration did not significantly affect the electrical conductivity (estimated as the reciprocal of impedance modulus, assuming solely ohmic contributions to the total impedance) of the thin films.

In a corresponding OCP measurement, a $Nb_{0.37}$ film was immersed for 45 min in 0.1 M HCl (Fig. S3a) prior to the conduction of EIS measurements analogous to those described above for 0.1 M H_2SO_4. The EIS results for the $Nb_{0.37}$ film in 0.1 M HCl indicated an analogous capacitive behavior as that seen in 0.1 M H_2SO_4. There was thus only a minor deviation (less than 4°) from the ideal case of a straight line parallel to the imaginary axis in the Nyquist plot while a phase angle of ca. 86° was found for frequencies below 10 Hz in the Bode phase plot. This indicates that the corrosion resistance of the $Nb_{0.37}$ film was comparable in 0.1 M H_2SO_4 and 0.1 M HCl under OCP conditions.

3.2.2. Potentiodynamic polarization curves recorded between − 0.7 and 3.0 V vs. Ag/AgCl (3 M NaCl)

After the OCP measurements, all films were scanned from − 0.7–3.0 V vs. Ag/AgCl (3 M NaCl). Fig. 4a shows the polarization curves for the nitrogen-containing $TiZrTaNb_y$ films with different Nb concentrations. In these curves, E_{corr} is found at the potential where the rate of the anodic reactions became equal to the rate of the cathodic reactions (i.e., $j_{an} = j_{cath}$) during the scan. In Fig. 4a, the E_{corr} values were found to be approximately − 0.13 V vs. Ag/AgCl (3 M NaCl) for all films and there was thus no significant dependence on the Nb concentration in the films. The different films also featured similar corrosion current densities j_{corr} between $3.2{\cdot}10^{-8}$ and $5.8{\cdot}10^{-8}$ A/cm^2. At potentials near 0.1 V vs. Ag/AgCl (3 M NaCl), the current densities were also similar for all films yielding values between $5.8{\cdot}10^{-8}$ and $1.35{\cdot}10^{-7}$ A/cm^2 at 0.25 V vs. Ag/AgCl (3 M NaCl). This indicates that the current densities seen in this potential range did not depend on the Nb concentrations in the films. A stable current density plateau (with current densities of around $5.5{\cdot}10^{-6}$ A /cm^2) was likewise seen for all the films above about 0.8 V vs. Ag/AgCl (3 M NaCl). This behavior is in good agreement with the findings of a previous study involving $(TiNbZrTa)N_x$ films with nitrogen concentration $x < 0.64$ [16]. Similar passive regions have also been observed for related HEAs systems such as TiTaNb [23] and HfNbTaTiZr [34].

Chart-bars showing the relative concentrations of the different elements found in the oxide layers prior to and after of the recording of the above-mentioned polarization curves are shown in Fig. 5a and

b, respectively. In these figures, different colors were used to depict the different elements and their relative intensities, i.e., Nb (yellow), Ta (mauve), Zr (green) and Ti (orange). The relative elemental ratios were obtained by fitting the high resolution XPS spectra shown in Fig. 2 and S4. The latter displays XPS spectra acquired from the nitrogen-containing $TiZrTaNb_y$ films prior to and after the recording of the polarization curves. The spectra are dominated by peaks corresponding to metal oxides, i.e., Nb_2O_5 at 207.3 eV, ZrO_2 at 182.3 eV, TiO_2 at 458.8 eV and Ta_2O_5 at 26.1 eV. In contrast to the spectra recorded from the pristine films (see Fig. 2), nitride peaks could not be seen after the recording of the polarization curves, indicating that the oxide thickness had increased. This observation is consistent with the high resolution XPS spectra recorded from a similar nitrogen containing $(TaTiZrNb)N_x$ film after scanning up to 4.0 V vs. Ag/AgCl (3 M NaCl) in 0.1 M H_2SO_4 [16]. After such scanning to 4.0 V vs. Ag/AgCl (3 M NaCl) the thickness of the oxide layer was found to be about 25–30 nm, i.e., significantly larger than the XPS probing depth, whereas the native oxide layer only had a thickness of a few nm according to literature values [16]. The XPS analyses of the native oxides also showed that the relative Nb concentration in the oxide layer increased with increasing the Nb content in the films (Fig. 5a). In addition, the relative ratios of all elements in the native oxide layer were close to the corresponding ratios in the bulk of the films (Fig. S5).

After having recorded the polarization curves shown in Fig. 4a, the relative Nb elemental concentrations remained similar to the relative intensities found in the native oxides (Fig. 5a and b). Significant increases in the Ta concentrations were, however, seen (Fig. 5b) for all films independent of the Nb concentration in the films. Lower relative concentrations were, consequently, seen for both Ti and Zr after recording polarization curves up to 3.0 V vs. Ag/AgCl (3 M NaCl). This indicates that the corrosion rate was higher for Ti and Zr than for Nb and lowest for Ta. Based on the observed Ta surface enrichment, Ta should hence be considered as the main passive element in the films. The analysis of the polarization curves obtained in 0.1 M H_2SO_4 therefore indicates that the presence of the native oxide led to polarization curves (Fig. 4a) with shapes that did not depend on the Nb concentration in films. More importantly, the results clearly show that the variation in the Nb concentration in the films had very little impact on the corrosion resistances of the films due to the fact that the films already had a sufficiently high concentration of Ta.

To further study the influence of the native oxide layer on the corrosion resistance of the films, a cathodic electrode pretreatment potential step (to −1.0 V vs. Ag/AgCl (3 M NaCl) for three minutes) was included prior to the recording of the polarization curves [5,10] for the $Nb_{0.19}$, $Nb_{0.25}$, $Nb_{0.31}$ and $Nb_{0.37}$ films. Fig. 6 shows a plot of the calculated charge (calculated by integrating the currents, see Fig. S6) associated with this potential step as a function of the Nb concentration in the films. As the reduction charges were found to be 47, 64, 105 and 140 mC/cm^2 for the $Nb_{0.19}$, $Nb_{0.25}$, $Nb_{0.31}$ and $Nb_{0.37}$ respectively, it is clear that there was an almost linear increase in the reduction charge when increasing the Nb concentration in the films.

The results shown in Fig. 6 hence indicate that a larger fraction of the native oxide layer was reduced for a film containing a higher concentration of Nb during the cathodic pre-treatment step. It is therefore reasonable to assume that the reduction involved a reduction of a Nb oxide such as Nb_2O_5. Since the standard potential for the reduction of Nb_2O_5 to Nb is − 0.8 V vs. Ag/AgCl (3 M NaCl), see the Supplementary Information, one would expect this reaction to take place at − 1.0 V vs. Ag/AgCl (3 M NaCl), assuming standard conditions (e.g., $[H^+]$ = 1.0 M). This also means that it is possible that there was a reduction of Nb_2O_5 in 0.1 M H_2SO_4 (and most likely also in 0.1 M HCl).

Following the cathodic pretreatment at − 1.0 V vs. Ag/AgCl (3 M NaCl), polarization curves were recorded from − 0.7–3.0 V vs. Ag/AgCl (3 M NaCl) for the $Nb_{0.19}$ and $Nb_{0.37}$ films. The results shown in Fig. 4b, demonstrate that the shape of the first part of the polarization curves was significantly altered with respect to the polarization curves seen in Fig. 4a, which were recorded without the cathodic pretreatment. This can be explained by the fact that some of the oxides (e.g., Nb_2O_5) in the passive layer most likely underwent reduction during the cathodic treatment as discussed above. The different shapes of the polarization curve recorded after the cathodic pretreatment step should hence reflect the electrochemical reactions needed to restore the passive layer.

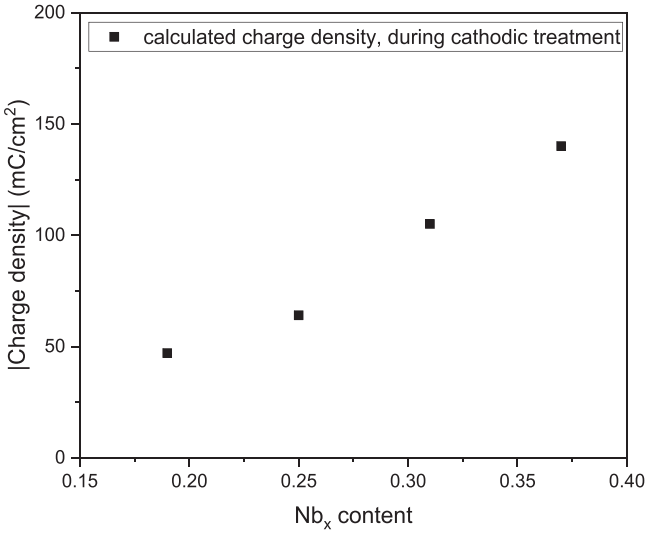

Fig. 6. Calculated charge density associated with the cathodic pre-treatment at − 1.0 V vs. Ag/AgCl (3 M NaCl) for three minutes as a function of the Nb concentration in the films in 0.1 M H_2SO_4.

The E_{corr} values, obtained after having used the cathodic pretreatment, were about − 0.23 V vs. Ag/AgCl (3 M NaCl), whereas the corrosion current densities j_{corr} were approximately 1×10^{-7} A/cm^2 for the $Nb_{0.19}$ and $Nb_{0.37}$ films. This means that the E_{corr} values in Fig. 4b were about 100 mV more negative compared to those in Fig. 4a. During the anodic scan, the current density increased to reach a stable value of about 5.5×10^{-6} A/cm^2, at ~1.3 V vs. Ag/AgCl (3 M NaCl) for the $Nb_{0.19}$ film, and at ~0.9 V vs. Ag/AgCl (3 M NaCl) for the $Nb_{0.37}$ film (Fig. 4b). The fact that the passivation was seen at a lower potential for the film with the higher Nb concentration indicates that Nb affected the kinetics of the surface re-passivation process. The results, on the other hand, also show that the Nb concentration did not affect the corrosion resistances of the films coated with more mature passive films significantly.

The latter conclusion is further supported by the fact that the XPS surface analysis of the surfaces of the cathodically treated $Nb_{0.19}$ and $Nb_{0.37}$ films, polarized up to 3.0 V vs. Ag/AgCl (3 M NaCl), did not show any significant differences depending on whether the cathodic treatment was used or not (Fig. 5b and c). In both cases (i.e., with and without the cathodic pretreatment step), lower relative intensities were seen for both Zr and Ti, while the Nb intensities were about the same as for the pristine films. As a result, the surfaces of the $Nb_{0.19}$ and $Nb_{0.37}$ films became enriched in Ta. This indicates that a stable passive layer (with approximately the same composition) was formed when scanning up to 3.0 V Ag/AgCl (3 M NaCl) with and without the cathodic pretreatment step.

A $Nb_{0.37}$ film was likewise cathodically treated at − 1.0 V vs. Ag/AgCl (3 M NaCl) for three minutes in 0.1 M HCl prior to the recording of a polarization curve as described above. From the polarization curves shown in Fig. 4b it can be seen that the obtained E_{corr} and j_{corr} values were very similar in 0.1 M HCl and 0.1 M H_2SO_4 (i.e., 8×10^{-8} A/cm^2 and −0.20 V in 0.1 M HCl compared to 6×10^{-8} A/cm^2 and −0.23 V

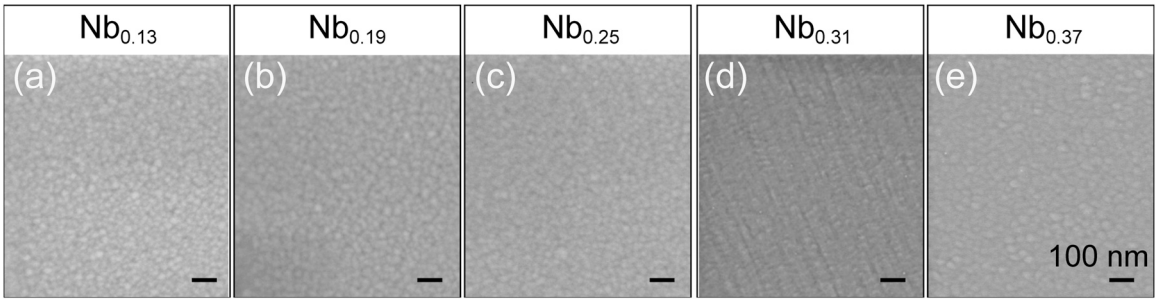

Fig. 7. SEM images of the nitrogen-containing $TiZrTaNb_y$ films after the recording of the polarization curves up to 3.0 V vs. Ag/AgCl (3 M NaCl) in 0.1 M H_2SO_4.

vs. Ag/AgCl (3 M NaCl) in 0.1 M H_2SO_4). At potentials above E_{corr} both polarization curves featured the same shape, and the passivation was also reached at almost the same potential, i.e., about 0.85 V vs. Ag/AgCl (3 M NaCl) after which a stable current of 5.3×10^{-6} A/cm^2 was seen up to 3.0 V vs. Ag/AgCl (3 M NaCl). Here it should be mentioned that a Zr film was found to start to undergo dissolution at about 0.5 V vs. Ag/AgCl (3 M NaCl) in 0.1 M HCl but not in 0.1 M H_2SO_4 (Fig. S7). For pure Nb, Ti and Ta electrodes an increase in the oxidation current was merely seen at about 2.1 V for the Ta and Ti electrodes and at about 2.5 V vs. Ag/AgCl (3 M NaCl) for the Nb electrode. The fact that the $Nb_{0.37}$ film retained a stable passive region in 0.1 HCl hence demonstrate that although Zr may corrode in 0.1 M HCl, a passive layer, was still obtained for the $Nb_{0.37}$ film. The similar relative intensity values seen for all elements in the XPS surface analyses after scanning to 3.0 V vs. Ag/AgCl (3 M NaCl) in 0.1 M HCl and 0.1 M H_2SO_4 (Fig. 5c), can thus be explained by the fact that the surfaces of the films became enriched in Ta and Nb. This finding, which explains the similar corrosion resistances seen for the $Nb_{0.37}$ films in 0.1 M HCl and 0.1 M H_2SO_4, clearly implies that Zr and Ti were lost from the surfaces of the film to about the same extent in both electrolytes.

After the anodic polarization up to 3.0 V vs. Ag/AgCl (3 M NaCl), no significant changes in the surface morphology were found for any of the $TiZrTaNb_y$ films (Fig. 7). The fine-grained feature observed for the pristine films was hence still visible even after the polarization. It is assumed from the results that a uniform corrosion type was mostly seen from the experiments which is in accordance with the absence of a pitting potential in the polarization curves. Therefore, a few pits could be seen in a low-magnification SEM images in some cases (Fig. S8) revealed the presence of larger surface defects prior to the corrosion experiments, which appeared to have been remained mostly unaffected by the recording of the polarization curve.

The results from this study have clearly shown that the Nb concentration in the films did not affect the corrosion resistance of the films. The XPS results show that the surfaces of all films became Ta-rich after of the recording of polarization curves up to 3.0 V in both 0.1 M HCl and 0.1 M H_2SO_4. This demonstrates that Ta played a significant role in the passivation process. Since the Ta concentration (i.e. about 15–19.5 ± 1.0 at%, see Table 1), remained almost stable in the composition of the different studied films (i.e. no significant Ta loss upon anodic polarization), the results indicate that the sum of the concentrations of Ta and Nb was always above the percolation threshold even for the lowest Nb concentration (i.e. about 8 at%, see Table 1). Although the different Nb concentrations in the films did not affect the overall corrosion resistance, the use of Nb as a second passivating element was still of high importance. By replacing Nb with Cr, the corrosion resistance of a film was found to decrease significantly as is described below. While morphological characterizations of these Nb or Cr containing films have been presented in a separate work [28], the corrosion resistances of the two films were not studied. Polarization curves for $TiTaZrCrN_{0.60}$ and $TiTaZrNbN_{0.60}$ films recorded in 0.1 M H_2SO_4 are, however, shown in Fig. S9. A corrosion current density of around $3 \cdot 10^{-8}$ A/cm^2 was observed for the Cr containing film whereas that for the Nb containing thin film was about $1.5\ 10^{-7}$ A/cm^2. The corresponding E_{corr} values were about 0.03 V and − 0.26 V vs. Ag/AgCl (3 M NaCl) for Nb and Cr containing films, respectively. Despite the lower corrosion current density and more positive corrosion potential obtained for the Cr containing film, indicating an improved corrosion resistance in the vicinity of E_{corr}, the polarization curve for the $TiTaZrCrN_{0.60}$ film showed a high current increase above about 1.45 V vs. Ag/AgCl (3 M NaCl). This is, however, not surprising as the corrosion protection offered by the Cr_2O_3 cannot be retained above 1.15 V vs. Ag/AgCl (3 M NaCl) due to the oxidation yielding soluble Cr(VI) species (e.g., $HCrO_4^-$, based on the reaction: $2\ HCrO_4^- + 6\ e^- + 8\ H^+ \leftrightarrow Cr_2O_3 + 5\ H_2O$ with E^0 =1.35 V vs. SHE (or at 1.15 V vs. Ag/AgCl (3 M NaCl)). For the Cr containing thin film it was, consequently, not possible to maintain the stable passive layer up to 3.0 V vs. Ag/AgCl (3 M NaCl) seen for the $TiTaZrNbN_{0.60}$ film (Fig. S9, green line), despite the fact that the Ta concentration was the same in both films. These results clearly show that the replacement of Nb with Cr results in a lower corrosion resistance at high potentials.

This study suggests that even though the different Nb concentrations in the thin films did not affect their corrosion resistance, the presence of a second passive element in the composition could still be of high significance. This is due to the fact that the presence of more than one passivating element in the composition could further improve the corrosion resistance, but it might also affect other parameters such as the production cost of an alloy, the mechanical or electrical properties [40,41]. The above results are important for perfecting the design of multicomponent thin films such as HEA-based compositions with improved corrosion properties.

3.2.3. Polarization curves recorded between − 0.7 and 0.45 V vs. Ag/AgCl (3 M NaCl) in 0.1 M H_2SO_4

To study the identity of the electrochemical behavior of the films seen at potentials lower than 0.8 V vs. Ag/AgCl (3 M NaCl) in Figs. 4a and 4b, polarization curves were also recorded between − 0.7 and 0.45 V vs. Ag/AgCl (3 M NaCl) in 0.1 M H_2SO_4 for a cathodically pretreated and an as-prepared $Nb_{0.31}$ film, respectively. From the data presented in Fig. 8a, it can be seen that the E_{corr} values were about − 0.3 V and − 0.18 V vs. Ag/AgCl (3 M NaCl) with and without the cathodic pretreatment step, respectively. The corresponding j_{corr} values were around $1.5 \cdot 10^{-7}$ A/cm^2 and $4.2 \cdot 10^{-8}$ A/cm^2. For the cathodically treated film, the oxidation current was more stable reaching approximately $5 \cdot 10^{-7}$ A/cm^2 at about 0.1 V vs. Ag/AgCl (3 M NaCl). The corresponding value without the cathodic pretreatments was lower, i.e., about $1 \cdot 10^{-7}$ A/cm^2. The observed difference can be attributed to the need to oxidatively restore the passive film after having reduced oxide, e.g., Nb_2O_5, present in the native passive layer during the cathodic pretreatment step. The results shown in Fig. 8 clearly show that the cathodic pretreatment step affected the electrochemical properties at potentials up to 0.45 V vs. Ag/AgCl (3 M NaCl) as the passive layer had to be restored after the cathodic

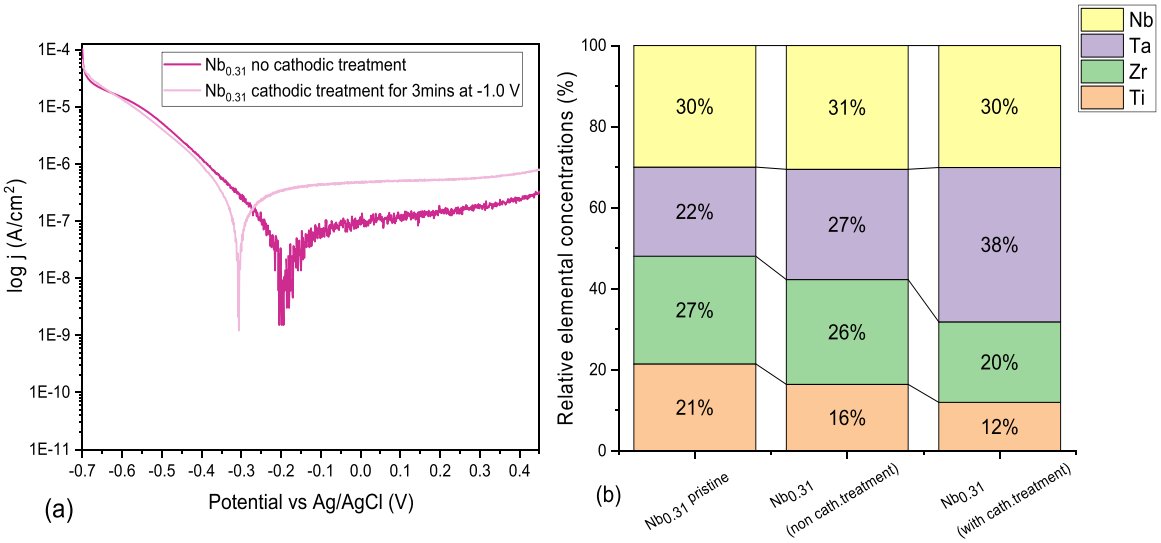

Fig. 8. Polarization curves recorded for the $Nb_{0.31}$ film in 0.1 M H_2SO_4 from − 0.7–0.45 V vs. Ag/AgCl (3 M NaCl) at room temperature using a scan rate of 1 mV/s, without (dark pink) and with (light pink) a cathodic treatment at − 1 V vs. Ag/AgCl (3 M NaCl) for three minutes (a). Relative elemental concentrations obtained by fitting the metal core levels of a $Nb_{0.31}$ pristine film (first column) and a $Nb_{0.31}$ film subjected to the recording of a polarization curve from − 0.7–0.45 V vs. Ag/AgCl (3 M NaCl) in the presence (second column), and absence (third column) of a cathodic pretreatment step (b).

pretreatment step. It is, however, important to note that this restoration of the passive layer was a time-dependent process, and the composition of the restored passive layer was very similar to that obtained in the absence of the cathodic pretreatment step. (i.e., samples scanned for higher potentials, see paragraph 3.2.2.).

Subsequent to the polarization experiments between − 0.7 and 0.45 V vs. Ag/AgCl (3 M NaCl), XPS was used to probe the surface composition of both $Nb_{0.31}$ films (Fig. 8b), and the thicknesses of the oxide layers were also determined by TEM (Fig. 9). The high-resolution XPS spectra (Fig. S10) showed that a mixture of oxides was present on the surface of the films and that the peaks could be assigned to Nb_2O_5, ZrO_2, TiO_2 and Ta_2O_5, in agreement with the results for the pristine films (Fig. 2). The TEM results indicated that the average oxide layer for the $Nb_{0.13}$ film obtained without any cathodic pre-treatment was thinner i.e., ~1.7 nm (Fig. 8) than the native oxide layer i.e., ~2.7 nm (Fig. 3a). After the cathodic treatment, the thickness of the oxide layer was, on the other hand thicker than the non-cathodically pretreated sample, i.e., about ~2.9 nm (Fig. 9). The latter finding is in accordance with the larger oxidation current seen in the polarization curve for the cathodically pretreated film (Fig. 8a). The limited growth of the oxide layer during the scan up to 0.45 V vs. Ag/AgCl (3 M NaCl) explains why nitride peaks also could be observed in the XPS high-resolution spectra (Fig. S10) since the probing depth of the XPS technique was about 5–10 nm [33].

The higher oxidation current seen in the polarization curve (Fig. 8a) for the cathodically treated film compared to the non cathodically treated film thus agrees with the lower relative ratio for Ti and Zr in Fig. 8b, indicating a faster etching of the latter two elements. The corrosion of Nb was rather limited compared to that for Ti and Zr but more pronounced than for Ta. The preferential loss of Ti and Zr hence resulted in a passive layer enriched in Ta, with a higher Ta relative intensity ratio for the cathodically treated film. The higher relative intensity for Ta along together with the lower intensities for Ti and Zr indicate that the preferential loss of Ti and Zr was facilitated by the cathodic pretreatments step. This resulted in an about 40% thicker Ta-rich passive layer for the cathodically treated film (Figs. 9a and 9b).

The results also show that the use of a cathodic pretreatment step, yielding a higher etching rate for Ti and Zr, resulting in higher currents (i.e., a lower corrosion resistance) at potentials up to 0.45 V vs. Ag/AgCl (3 M NaCl) as a result of the need to restore the disturbed passive layer.

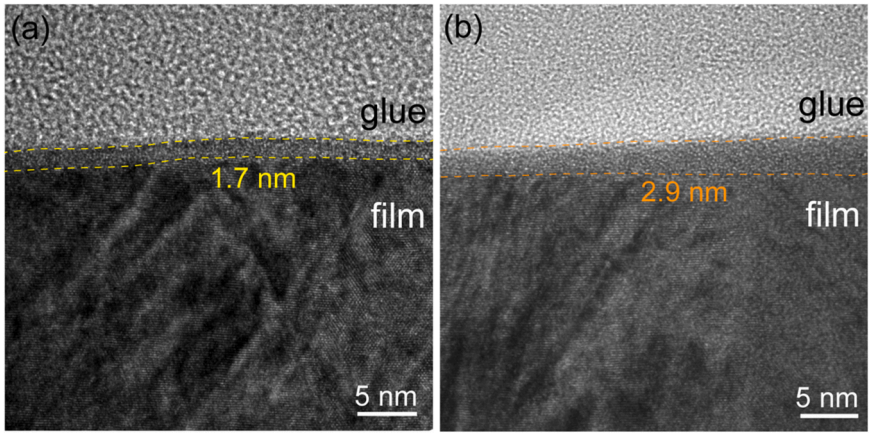

Fig. 9. TEM image acquired near the film surface region for the non-cathodically pretreated (a) and the cathodically pretreated $Nb_{0.31}$ film (b) after the recording of a polarization curve from − 0.7 0.45 V vs. Ag/AgCl (3 M NaCl) in 0.1 M H_2SO_4.

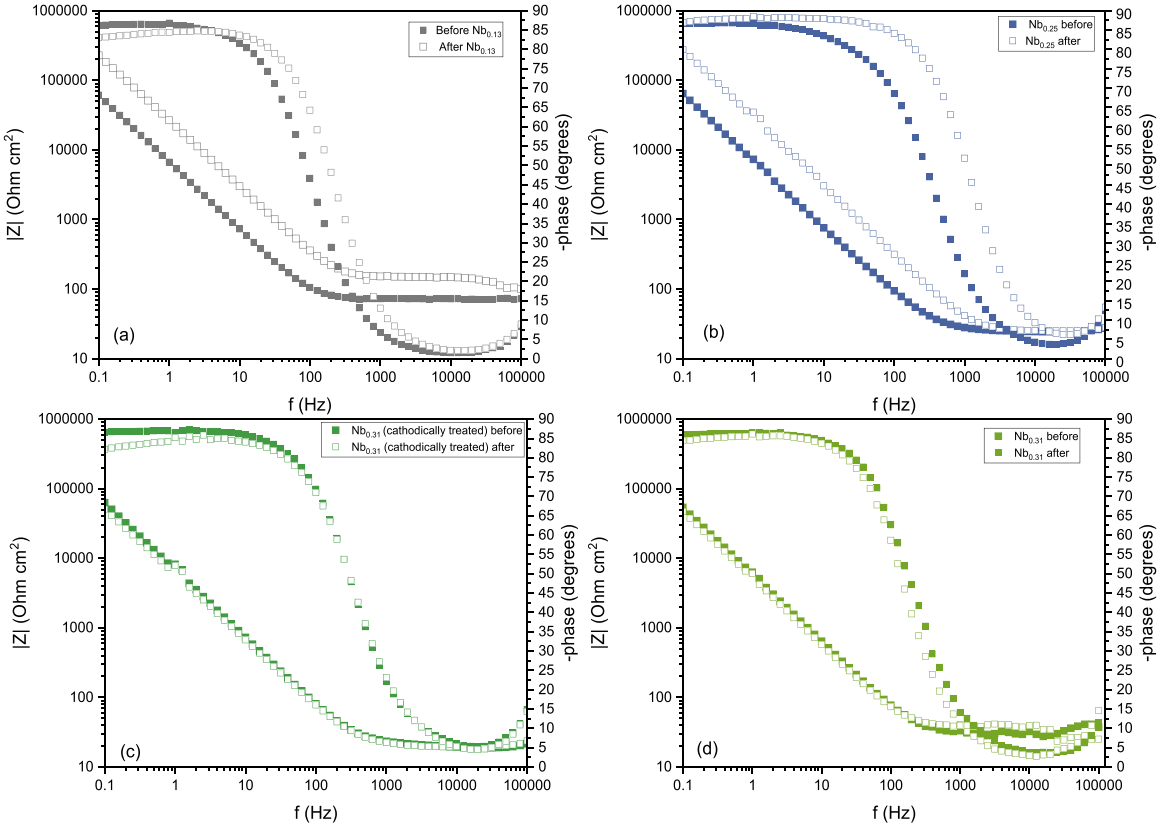

Fig. 10. Electrochemical impedance data, obtained under OCP conditions, presented as Bode phase and magnitude plots before (full color filled squares) and after the recording of polarization curves (empty color filled squares). The EIS data were measured for a $Nb_{0.13}$ (a) and $Nb_{0.25}$ (b) film scanned from − 0.7–3.0 V vs. Ag/AgCl (3 M NaCl) and two $Nb_{0.31}$ films (c and d) scanned up to 0.45 V vs. Ag/AgCl (3 M NaCl) in the presence (c) and absence (d) of a cathodic pretreatment step (i.e., −1.0 V vs. Ag/AgCl (3 M NaCl for three minutes).

3.2.4. Electrochemical impedance spectroscopy after anodic polarization in 0.1 M H_2SO_4

The EIS data were recorded under OCP conditions after the recording of polarization curves up to 0.45 V vs. Ag/AgCl (3 M NaCl) for the $Nb_{0.31}$ films, with and without the cathodic pretreatment step. EIS data were also recorded under OCP conditions after the recording of polarization curves up to 3.0 V vs. Ag/AgCl (3 M NaCl) for both $Nb_{0.13}$ and $Nb_{0.25}$ films.

As seen in the Nyquist plots in Fig. S11a, a capacitive-like behavior was seen before and after the recording of the polarization curves in agreement with the results for the pristine $Nb_{0.31}$ film. The inset of Fig. S11a shows the impedance values for the $Nb_{0.31}$ films at a higher magnification. The electronic resistance of the films before and after the polarization to 0.45 V vs. Ag/AgCl (3 M NaCl) was estimated following the approach applied for the pristine materials (see Section 2.1). From the data presented in Fig. S11b, minor variations in the high frequency resistance are seen, suggesting a negligible effect of the anodic polarization treatment (up to 3.0 V vs. Ag/AgCl (3 M NaCl)) on the electronic properties of the composites.

To provide further insights into the effect of anodic polarization on the structural properties of the films an estimation of the electrochemically active surface area (ECSA) was made based on the assumption that the ECSA value should be affected by changes in the surface morphology of the films (e.g., variations in the porosity). A change in the ECSA should result in a change in the capacitance, C, of the interface since the capacitance should be proportional to the ECSA. The capacitance values were extracted from the EIS data presented in Fig. 10, using the approach reported by Pickup et al. [42,43]. This approach involves plotting the parameter $-1/(2\pi fImZ)$ (representing the capacitance of the interface) vs. ReZ. From such plots, the limiting capacitance value, C_{lim}, can be approximated by the plateau of the $-1/(2\pi fImZ)$ parameter often seen in the low frequency range. The C_{lim} value corresponds to the frequency range within which the penetration length of the ac signal is equal to or higher than the penetration depth of the electrolyte which means that the entire ECSA is probed. In this approach, it is assumed that the interface exhibits a blocking behavior at low frequencies and that the reactance of the system therefore is solely attributed to the double layer capacitance. This assumption should be valid here given the phase angle values (> 85°) seen in the Bode phase plots in Fig. 10. From the results presented in Figs. S12 and S13, it can be deduced that C_{lim} values for the $Nb_{0.13}$ and $Nb_{0.25}$ films decreased by a factor of about four as a result of their scanning up to 3.0 vs. Ag/AgCl (3 M NaCl), but for the $Nb_{0.31}$ films scanned up to 0.45 V vs. Ag/AgCl (3 M NaCl) a slight increase by a factor of ca. 1.2 was instead seen. The small difference in C_{lim} seen for the $Nb_{0.31}$ films indicates that any changes in the morphology of the oxide layer did not have a significant impact on the ECSA of the composites upon polarization to 0.45 V vs. Ag/AgCl (3 M NaCl)). Therefore, minor changes are expected on the overall morphological characteristics (i.e., porosity, thickness) of the surface oxide layer. This is supported by TEM investigations on the non-cathodically pretreated (Fig. 9a) and cathodically pretreated (Fig. 9b) $Nb_{0.31}$ films after polarization to 0.45 V vs. Ag/AgCl (3 M NaCl)), which demonstrate the formation of a very thin (less than 3 nm thick) oxide layer, with a morphology similar to that of the pristine film. This means that the minor increase in C_{lim} (and hence ECSA) indicated by the EIS results can be attributed to the thin surface oxide layer formed during the initial stages of the polarization (see Fig. 8a) as this would alter the roughness factor of the film to some extent. The observed significant decrease in C_{lim} for the $Nb_{0.13}$ and $Nb_{0.25}$ films following anodic polarization up to 3.0 V vs. Ag/AgCl (3 M NaCl), can, on the other hand, be ascribed to the formation of a much thicker and compact oxide layer. The presence of oxide layers with thicknesses of more than 25 nm, previously

reported for films with similar compositions upon polarization in this potential range [16], have been ascribed to a 3D oxide network growth decreasing the overall porosity of the oxide layers.

4. Conclusions

Nitrogen-containing $TiZrTaNb_y$ films, with Nb concentrations between 8.0.0 at% and 24.5 at%., were synthesized by magnetron sputtering to study the influence of the Nb concentration on the corrosion resistances of the films. The results of the electrochemical measurements, including the recording of polarization curves and electrochemical impedance spectroscopy experiments showed that all films exhibited an almost stable current plateau between 0.8 and 3.0 V vs. Ag/AgCl (3 M NaCl). Despite the significant change in the Nb concentration, the corrosion resistances of the films remained essentially unaffected in both 0.1 M H_2SO_4 and 0.1 M HCl. This effect is ascribed to the formation of a passive layer enriched in Ta and Nb as a result of the fact that the sum of the Ta and Nb concentration was high enough to ensure good passivation even for the lowest Nb concentration. During the recording of the polarization curves, the passive layer was found to become enriched in Ta, whereas Ti and Zr were preferentially lost from the surfaces of the films. This loss of Ti and Zr was proven by XPS analyses of the surfaces of the films. Although some Nb was detected by XPS means, on the film surfaces, its presence had no significant influence for the corrosion resistance of the thin films, due to the high Ta concentration in the films. The results hence indicate that the employed Ta concentration (i.e., 15–19.5 at%) allows passivation of the films even if the Nb concentration is decreased to 8.0 at%. The introduction of a cathodic pretreatment step at − 1.0 V vs. Ag/AgCl (3 M NaCl) for three minutes was found to impact the E_{corr} and j_{corr} values, as well as the oxidation currents seen at potentials lower than 0.8 V vs. Ag/AgCl (3 M NaCl). The cathodic pretreatment did, however, not affect the electrochemical performance, of films scanned up to 3.0 V vs. Ag/AgCl (3 M NaCl). The XPS and TEM analyses indicate that the cathodic pretreatment step resulted in an enhanced preferential loss of Ti and Zr from the surface of the films yielding a form a thicker Ta-rich passive layer compared to for a non-cathodically treated film when only scanning up to 0.45 V vs. Ag/AgCl (3 M NaCl). Although there was no significant influence of the Nb concentration in the films on the overall corrosion resistance, the presence of Nb was still important. When replacing Nb with Cr a low corrosion resistance was observed at high potentials due to the onset of the Cr transpassive region at about 1.45 V vs. Ag/AgCl (3 M NaCl). These results pave the way for the design of new highly corrosion-resistant multicomponent thin films, comprising more than one passivating element.

CRediT authorship contribution statement

Eirini-Maria Paschalidou Conceptualization, Investigation, Formal analysis, Writing – original draft. **Rui Shu** Conceptualization, Investigation, Formal analysis, Writing – original draft. **Robert Boyd** Investigation, Formal analysis. **Athanasios A. Papaderakis** Formal analysis, Writing – original draft. **Babak Bakhit** Investigation, Formal analysis. **Arnaud le Febvrier** Supervision, Writing – review & editing. **Grzegorz Greczynski** Investigation, Formal analysis, Writing – review & editing, **Per Eklund** Supervision, Project administration, Funding acquisition, Writing – review & editing. **Leif Nyholm** Supervision, Conceptualization, Writing – review & editing.

Data Availability

Data will be made available on request.

Declaration of Competing Interest

The authors declare that they have no known competing financial interests or personal relationships that could have appeared to influence the work reported in this paper.

Acknowledgments

This study was performed within the framework of the competence center FunMat-II that is financially supported by Vinnova (grant no. 2016-05156). B Bakhit gratefully acknowledges financial support from Swedish Research Council (VR), (grant no. 2021-00357). Also, the Knut and Alice Wallenberg Foundation is acknowledged through the Wallenberg Academy Fellows program (grant no. KAW 2020.0196) and the Swedish Research Council (VR) under project grant no. 2021-03826. We acknowledge Uppsala University and Myfab Uppsala for providing facilities and experimental support. Myfab is funded by the Swedish Research Council (2019-00207) as a national research infrastructure."

Appendix A. Supporting information

Supplementary data associated with this article can be found in the online version at doi:10.1016/j.jallcom.2022.167005.

References

[1] M. Pourbaix, Atlas of electrochemical equilibria in aqueous solutions, Natl. Assoc. Corros. Eng. (1974).
[2] A. Atrens, B. Baroux, M. Mantel, The secondary passive film for type 304 stainless steel in 0.5 M H_2SO_4, J. Electrochem. Soc. 144 (1997) 3697, https://doi.org/10.1149/1.1838078
[3] I. Betova, M. Bojinov, T. Laitinen, K. Mäkelä, P. Pohjanne, T. Saario, The transpassive dissolution mechanism of highly alloyed stainless steels: I. Experimental results and modelling procedure, Corros. Sci. 44 (2002) 2675–2697, https://doi.org/10.1016/S0010-938X(02)00073-2
[4] K. Sieradzki, R. Newman, A percolation model for passivation in stainless steels, J. Electrochem Soc. 133 (1986) 1979–1980, https://doi.org/10.1149/1.2109065
[5] Y. Xie, D.M. Artymowicz, P.P. Lopes, A. Aiello, D. Wang, J.L. Hart, E. Anber, M.L. Taheri, H. Zhuang, R.C. Newman, K. Sieradzki, A percolation theory for designing corrosion-resistant alloys, Nat. Mater. 20 (2021) 789–793, https://doi.org/10.1038/s41563-021-00920-9
[6] R.C. Newman, S.G. Corcoran, J. Erlebacher, M.J. Aziz, K. Sieradzki, Alloy corrosion, MRS Bull. 24 (1999) 24–28, https://doi.org/10.1557/S0883769400052660
[7] S. Qian, R.C. Newman, R.A. Cottis, K. Sieradski, Computer passivation of alloy passivation and activation, Corros. Sci. (1990) 621–626, https://doi.org/10.1016/0010-938X(90)90171-Z
[8] M. Liu, A. Aiello, Y. Xie, K. Sieradzki, The effect of short-range order on passivation of Fe-Cr alloys, J. Electrochem. Soc. 165 (2018) C830–C834, https://doi.org/10.1149/2.0871811jes
[9] A. Aiello, Corrosion and passivation of Mg-Al and Ni-Cr alloys, ASU, Doctoral dissertation, Academic thesis, (2018), https://hdl.handle.net/2286/R.I.51583.
[10] S. Fujimoto, R.C. Newman, G.S. Smith, S.P. Kaye, H. Kheyrandish, J.S. Colligon, Corros. Sci. 35 (1-4) (1993) 51–55, https://doi.org/10.1016/0010-938X(93)90132-Z
[11] E. Lewin, Multi-component and high-entropy nitride coatings—A promising field in need of a novel approach, J. Appl. Phys. 127 (2020) 160901, https://doi.org/10.1063/1.514415
[12] C. Oses, C. Toher, S. Curtarolo, High-entropy ceramics, Nat. Rev. Mater. 5 (4) (2020) 295–309, https://doi.org/10.1038/s41578-019-0170-8
[13] D.B. Miracle, O.N. Senkov, A critical review of high entropy alloys and related concepts, Acta Mater. 122 (2017) 448–511, https://doi.org/10.1016/j.actamat.2016.08.081
[14] D. Moskovskikh, S. Vorotilo, V. Buinevich, A. Sedegov, K. Kuskov, A. Khort, C. Shuck, M. Zhukovskyi, A. Mukasyan, Extremely hard and tough high entropy nitride ceramics, Sci. Rep. 10 (2020) 19874, https://doi.org/10.1038/s41598-020-76945-y
[15] A. Srinath, K. von Fieandt, R. Lindblad, S. Fritze, M. Korvela, J. Pettersson, E. Lewin, L. Nyholm, Influence of the nitrogen content on the corrosion resistances of multicomponent AlCrNbYZrN coatings, Corros. Sci. 188 (2021) 109557, https://doi.org/10.1016/j.corsci.2021.109557
[16] R. Shu, E.-M. Paschalidou, S.G. Rao, B. Bakhit, R. Boyd, M.V. Moro, D. Primetzhofer, G. Greczynski, L. Nyholm, A. le Febvrier, P. Eklund, Effect of nitrogen content on microstructure and corrosion resistance of sputter-deposited multicomponent (TiNbZrTa)N_x films, Surf. Coat. Technol. 404 (2020) 126485, https://doi.org/10.1016/j.surfcoat.2020.126485
[17] R. Shu, E.-M. Paschalidou, S.G. Rao, J. Lu, G. Greczynski, E. Lewin, L. Nyholm, A. le Febvrier, P. Eklund, Microstructure and mechanical, electrical, and

electrochemical properties of sputter-deposited multicomponent (TiNbZrTa)N_x coatings, Surf. Coat. Technol. 389 (2020) 125651https://doi.org/10/ggqssx.
[18] K. von Fieandt, E.-M. Paschalidou, A. Srinath, P. Soucek, L. Riekehr, L. Nyholm, E. Lewin, Multi-component (Al,Cr,Nb,Y,Zr)N thin films by reactive magnetron sputter deposition for increased hardness and corrosion resistance, Thin Solid Films 693 (2020) 137685, https://doi.org/10.1016/j.tsf.2019.137685
[19] T. Wirtanen, T. Prenzel, J.-P. Tessonnier, S.R. Waldvogel, Cathodic corrosion of metal electrodes—How to prevent it in electroorganic synthesis, Chem. Rev. 121 (2021) 10241–10270, https://doi.org/10.1021/acs.chemrev.1c00148
[20] H. Tawfik, Y. Hung, D. Mahajan, Metal bipolar plates for PEM fuel cell—A review, J. Power Sources 163 (2007) 755–767 //doi.org/10.1016/j.jpowsour.2006.09.088.
[21] Łukasz Kolanowski Jarosław Wojciechowski, Grzegorz Lota Andreas Bund, The influence of current collector corrosion on the performance of electrochemical capacitors, J. Power Sources 368 (2017) 18–29, https://doi.org/10.1016/j.jpowsour.2017.09.069
[22] Morten S. Jellesen, Daniel Minzari, Umadevi Rathinavelu, Per Møller, Rajan Ambat, Corrosion failure due to flux residues in an electronic add-on device, Eng. Fail. Anal. 17 (2010) 1263–1272, https://doi.org/10.1016/j.engfailanal.2010.02.010
[23] W.Y. Chen, Y.H. Chen, W.P. Li, R. Zhou, T.H. Chou, X. Wang, J.C. Huang, Passivation evolution of Ti-Ta-Nb medium-entropy sputtered thin films in sulfuric acid solution, Appl. Surf. Sci. 576 (2022) 151824, https://doi.org/10.1016/j.apsusc.2021.151824
[24] Z. Wang, Y. Yan, Y. Wu, X. Huang, Y. Zhang, Y. Su, L. Qiao, Corrosion and tribo-corrosion behavior of equiatomic refractory medium entropy TiZr(Hf, Ta, Nb) alloys in chloride solutions, Corros. Sci. 199 (2022) 110166, https://doi.org/10.1016/j.corsci.2022.110166
[25] A. le Febvrier, L. Landälv, T. Liersch, D. Sandmark, P. Sandström, P. Eklund, An upgraded ultra-high vacuum magnetron-sputtering system for high-versatility and software-controlled deposition, Vacuum 187 (2021) 110137, https://doi.org/10.1016/j.vacuum.2021.110137
[26] I. ISO, 15472: 2010 Surface chemical analysis—X-ray photoelectron spectrometers—calibration of energy scales, ISO Geneva Switz. (2010).
[27] G. Greczynski, L. Hultman, X-ray photoelectron spectroscopy: Towards reliable binding energy referencing, Prog. Mater. Sci. 107 (2020) 100591https://doi.org/10/gf8r7j.
[28] R. Shu, D. Lundin, B. Xin, M.A. Sortica, D. Primetzhofer, M. Magnuson, A. le Febvrier, P. Eklund, Influence of metal substitution and ion energy on microstructure evolution of high-entropy nitride (TiZrTaMe)N_{1-x} (Me = Hf, Nb, Mo, or Cr) films, ACS Appl. Electron, Mater 3 (2021) 2748–2756, https://doi.org/10.1021/acsaelm.1c00311
[29] K.S. Havey, J.S. Zabinski, S.D. Walck, The chemistry, structure, and resulting wear properties of magnetron-sputtered NbN thin films, Thin Solid Films 303 (1997) 238–245 https://doi.org/10/fdtnhk.
[30] P. Lackner, Z. Zou, S. Mayr, U. Diebold, M. Schmid, Using photoelectron spectroscopy to observe oxygen spill over to zirconia, Phys. Chem. Chem. Phys. 21 (2019) 17613–17620 https://doi.org/10/ggzv6p.
[31] P.J. Martin, R.P. Netterfield, T.J. Kinder, L. Descôtes, Deposition of TiN, TiC, and TiO2 films by filtered arc evaporation, Surf. Coat. Technol. 49 (1991) 239–243 https://doi.org/10/cxrp9d.
[32] J.A. Wilks, N.P. Magtoto, J.A. Kelber, V. Arunachalam, Interfacial reactions during sputter deposition of Ta and TaN films on organosilicate glass: XPS and TEM results, Appl. Surf. Sci. 253 (2007) 6176–6184 https://doi.org/10/cqr2jz.
[33] S. Tanuma, C.J. Powell, D.R. Penn, Calculations of electron inelastic mean free paths. IX. Data for 41 elemental solids over the 50 eV to 30 keV range, Surf. Interface Anal. 43 (2011) 689–713, https://doi.org/10.1002/sia.3522
[34] Q. Zhou, S. Sheikh, P. Ou, D. Chen, Q. Hu, S. Guo, Corrosion behavior of Hf0.5Nb0.5Ta0.5Ti1.5Zr refractory high-entropy in aqueous chloride solutions, Electrochem. Commun. 98 (2019) 63–68, https://doi.org/10.1016/j.elecom.2018.11.009
[35] M.K. Bahl, ESCA studies of some niobium compounds, J. Phys. Chem. Solids 36 (1975) 485–491, https://doi.org/10.1016/0022-3697(75)90132-8
[36] H. Höchst, R.D. Bringans, P. Steiner, Th Wolf, Photoemission study of the electronic structure of stoichiometric and substoichiometric TiN and ZrN, Phys. Rev. B 25 (1982) 7183–7191, https://doi.org/10.1103/PhysRevB.25.7183
[37] G. Greczynski, S. Mráz, J.M. Schneider, L. Hultman, Native target chemistry during reactive dc magnetron sputtering studied by ex-situ x-ray photoelectron spectroscopy, Appl. Phys. Lett. 111 (2017) 021604, https://doi.org/10.1063/1.4993787
[38] J.F. Moulder, W.F. Stickle, P.E. Sobol, K.D. Bomben, Perkin Elmer Corp. "Handbook of X-Ray Photoelectron Spectroscopy," Physical Electronics Division, Perkin-Elmer Corp., Norwalk, 1995.
[39] G. Greczynski, D. Primetzhofer, J. Lu, L. Hultman, Core-level spectra and binding energies of transition metal nitrides by non-destructive x-ray photoelectron spectroscopy through capping layers, Appl. Surf. Sci. 396 (2017) 347–358, https://doi.org/10.1016/j.apsusc.2016.10.152
[40] Q. Sui, L. Meng, S. Wang, P. Li, X. Yin, L. Wang, Effect of Nb addition on mechanical properties and corrosion behavior of Ti6Al4V alloy produced by selective laser melting, J. Mater. Res 35 (2022) (2020) 571–579, https://doi.org/10.1557/jmr.2019.415
[41] X. Guo, Z. Xiao, W. Qiu, Z. Li, Z. Zhao, X. Wang, Y. Jiang, Microstructure and properties of Cu-Cr-Nb alloy with high strength, high electrical conductivity and good softening resistance performance at elevated temperature, Mater. Sci. Eng. A 749 (2019) 281–290, https://doi.org/10.1016/j.msea.2019.02.036
[42] E.B. Easton, P.G. Pickup, An electrochemical impedance spectroscopy study of fuel cell electrodes, Electro Acta 50 (2005) 2469–2474, https://doi.org/10.1016/j.electacta.2004.10.074
[43] O.'R. Reid, F.S. Saleh, E.B. Easton, Determining electrochemically active surface area in PEM fuel cell electrodes with electrochemical impedance spectroscopy and its application to catalyst durability, Electrochim. Acta 114 (2013) 278–284, https://doi.org/10.1016/j.electacta.2013.10.050